Article

Experimental Investigation on Synergetic Effects of Micro Grooves and WSe₂ in Sliding Contact

Yuan Wei [1,*,†] (ID)**, Shuang Li** [1,†]**, He Huang** [1]**, Chongliang Ding** [2] **and Xuewen Wang** [1,*] (ID)

1   Frontiers Science Center for Flexible Electronics, Xi'an Institute of Flexible Electronics (IFE) and Xi'an Institute of Biomedical Materials & Engineering, Northwestern Polytechnical University, Xi'an 710072, China
2   Weinan WoodKing Intelligent Technology Co., Ltd., Weinan 714000, China
*   Correspondence: iamywei@nwpu.edu.cn (Y.W.); iamxwwang@nwpu.edu.cn (X.W.)
†   These authors contributed equally to this work.

Abstract: Improving tribological behaviors for dry contacts has always been a hot study topic, since liquid lubricants are not applicable for certain vital scenarios, including space travel equipment. This study describes the synergetic effects of micro groove texture and WSe₂ flakes as solid lubricants on friction reduction in dry sliding contact. The reciprocating sliding tests were performed under the dry and WSe₂ flake-filled conditions while varying the texture geometric feathers and WSe₂ flake sizes. According to the experimental results, the coefficient of friction (CoF) could be reduced by 80% due to the combination of micro grooves and WSe₂ flakes compared to the non-textured cases. The optimal width ($b = 130$ μm) of the groove was identified under both dry and WSe₂ flake-filled conditions. The SEM observation suggested that the WSe₂ flakes have different sizes. The influence of the WSe₂ granularity on reducing friction was discussed based on the results. This study provides a novel solution for reducing friction, which suggests that there is a synergetic effect and optimal parameters for friction reduction with micro grooves and WSe₂ flakes.

Keywords: micro groove; tungsten diselenide; geometrical features; friction reduction

1. Introduction

Friction and wear are vital concerns in any mechanical system [1]. Improving the lubrication condition of the mechanical system would make a significant contribution to the sustainable development goals [2–5], as nearly one-fifth of the world's energy consumption is due to friction and wear [6–8]. Using lubricants is the easiest solution to reduce friction and wear, [9]. Liquid lubricants are unsuitable in some special situations because of chemical decomposition or oxidation, harmful constituents, and other limitations [2,10–14]. In addition, the surface texture filled with solid lubricants could further reduce friction under dry friction conditions, and there are multiple approaches that can be used to deposit solid lubricants on the sample surface [9,15,16].

Several decades ago, many studies were performed to investigate the surface texture performance and its mechanism. Suh et al. [17] determined that the textured surface obtained outstanding tribological properties to reduce friction and wear compared with the smooth surface. The study also proposed that the geometry of undulations could be optimized to avoid negative effects on the tribological properties of samples. The results of Yan et al. [18] showed that the dimple pattern with a diameter of 100–200 μm, depth of 5–10 μm, and area ratio of 5% is optimal for lower friction in the research, and the study also indicated that the dimple area ratio is the most critical parameter to reduce the coefficient of friction (CoF). Xing et al. [19] researched the tribological properties of textured and smooth samples through a sliding wear test under dry friction condition. Compared with the smooth surface, the textured surface showed excellent tribological properties. Sun et al. [20] examined the tribological properties of textured and untextured surfaces by a dry sliding wear test. The results indicated that the wear volume of the textured surface could reduce

by half compared with the untextured surface, and the small diameter and high density of micro-dimples in samples could improve the wear resistance properties. Kumar et al. [21] studied the effect of a textured surface on the tribological properties of bearing steel under dry friction conditions. The results showed that the CoF of a sample is decreased compared with an untextured sample. A widely accepted mechanism indicates that the surface texture could reduce the real contact area and entrap the wear debris [19–28].

The excellent tribological properties of layered materials arise from their unique structure [2,9,29,30]. Layered materials are composed of single or few atomic or molecular layers, which are connected by strong covalent bonds or ionic bonds, while the interlayers are combined by weak van der Waals forces [2,31]. Voevodin et al. [32] filled grooves with MoS_2 on a TiC/DLC disk. The results suggested that the three-dimensional coating could reduce friction and improve wear resistance. Rapoport et al. [33] researched the effect of the density of dimples and the height of bulges around the textures on the life of the solid lubricant films. The study also revealed the effect of the depth of the textures on the wear life of MoS_2 film on textured surfaces. Deng et al. [34] compared the tribological properties of conventional tools and self-lubricated tools, which have micro-holes filled with MoS_2, by cutting tests under dry friction conditions. The results showed that the self-lubricated tools demonstrated better tribological properties. Hu et al. [35] proposed that the wear life of a MoS_2 solid lubricant coating could be improved by combining texturing and hot pressing. The study also demonstrated that the wear life of the textured surface is prolonged with the increase in the density of textures with hot pressed coating; the recommended optimum dimple density is 15–25%. Reinert et al. [36] used a ball-on-disk tribometer in linear reciprocating sliding mode to compare the effect of the combination of surface texture and carbon nanotubes (CNTs), and one of them on the tribological performance under dry friction conditions. The combined method could prolong lubrication life and reduce surface texture degeneration. Meng et al. [37] researched the tribological performance improvement of cemented carbides by combining laser surface texturing and WSC solid lubricant coating. The results suggested that the samples with the WSC solid lubricant coating and textured surfaces have more excellent tribological properties than others. In terms of the mechanism of the surface texture filled with layered materials, it is reported that the texture acts as a reservoir of wear debris and solid lubricants, and decreases the contact area of the friction pair, which make sliding easy [9,38–41]. However, the current studies on the synergetic effects of surface texturing and solid lubricants solely focus on layered sulfide-based materials and graphene [9]. The interactions between texture features and solid lubricants are still in need of further study. The mechanical characteristics of the combination of several ingredients mainly depend on the component which has high corresponding performance, the increase in the modulus of elasticity, and the Young's modulus of the composite material, due to the fact that the modulus of elasticity and the Young's modulus of the fillers are higher than the matrix [42,43]. It is necessary to understand the factors that may affect the synergetic effects of surface texturing and solid lubricants.

In this study, reciprocating sliding tests were performed under the dry and WSe_2 flake-filled conditions separately to investigate the texture geometrical features' influence on the synergetic effects of the micro groove texture and solid lubricant. The influence of varying micro groove widths, densities, and solid lubricant sizes on the synergetic effects of tribological properties was investigated. The results suggest that the combination of micro grooves and WSe_2 flakes could further enhance the friction reduction. The optimal width of the micro groove could be identified. The effect of the WSe_2 granularity on friction reduction was discussed based on results.

2. Samples Preparation

In the experiment, a low-carbon steel block (30 mm × 15 mm × 5 mm) was prepared as the sample. Figure 1 shows the sample preparation process, including the texturing and lubricant filling. A nanosecond laser was used to fabricate the micro grooves on the

sample surface with the laser output set at 8 W, laser wavelength = 1064 nm, laser spot diameter = 50 μm, laser pulse width <20 ns, and spot moving speed = 2000 mm/s. After the texturing, the sample was polished again to remove the asperities that were generated in the texturing process (Figure 1). Then, the samples were rinsed with acetone (20 min) in an ultrasonic cleaner. Micro grooves with different widths and densities on the samples were prepared separately for comparison. This is shown in Figure 2a,b, where b indicates the width of the micro groove and D indicates the inter-groove distance. The textured surfaces were observed using a white light interferometer to obtain the surface profile (NanoMap-1000WLI, AEP), which is shown in Figure 2b, and the line profile of the groove is shown in Figure 2c (red line on the surface profile). The surface roughness of the untextured surface S_a was 0.11 μm.
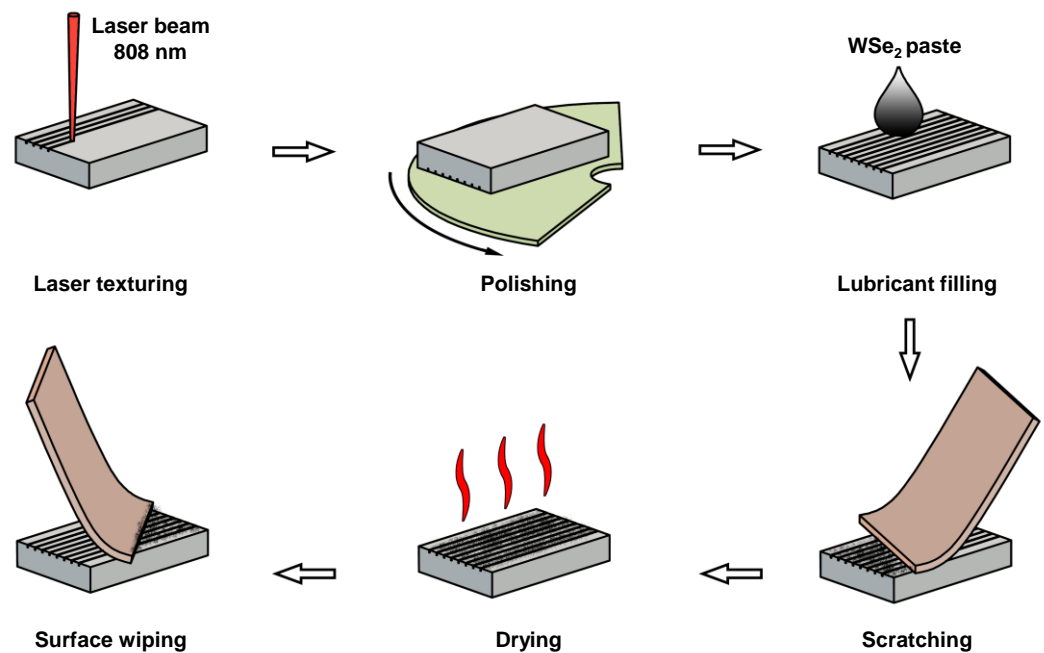

Figure 1. Procedures of samples preparation.

Tungsten diselenide (WSe$_2$) is selected as the lubricant for filling the micro grooves, which is one of the typical layered materials. Compared to the widely used layered solid lubricating materials, such as MoS$_2$ and WS$_2$, WSe$_2$ also has a relatively low exfoliation energy [44]. The bulk WSe$_2$ that was obtained using chemical vapor deposition was dispersed in the solution of deionized water/isopropyl alcohol (55 vol.%/45 vol.%) and sonicated at 540 W using a tip sonicator for 4 h at a constant temperature of 15 °C. Furthermore, the dispersion was centrifuged for 30 min to collect the supernatant and to remove unexfoliated WSe$_2$. Different sizes of WSe$_2$ flakes could be obtained from the precipitates collected at different rotational speeds of the centrifuge. Figure 3a shows the WSe$_2$ solution obtained after the centrifugation process. Then, the WSe$_2$ solution was freeze-dried using liquid nitrogen. The Raman test was performed to verify that the solution's main ingredient is WSe$_2$. The Raman spectrum (as shown in Figure 3a) has two characteristic peaks near 249 cm^{-1} and 261 cm^{-1}, which are the in-plane vibrational modes (E_{2g}^1) of the two Se atoms and the middle W atom, and these are perpendicular to the plane vibrational mode (A_{1g}) of the corresponding Se atom [45].
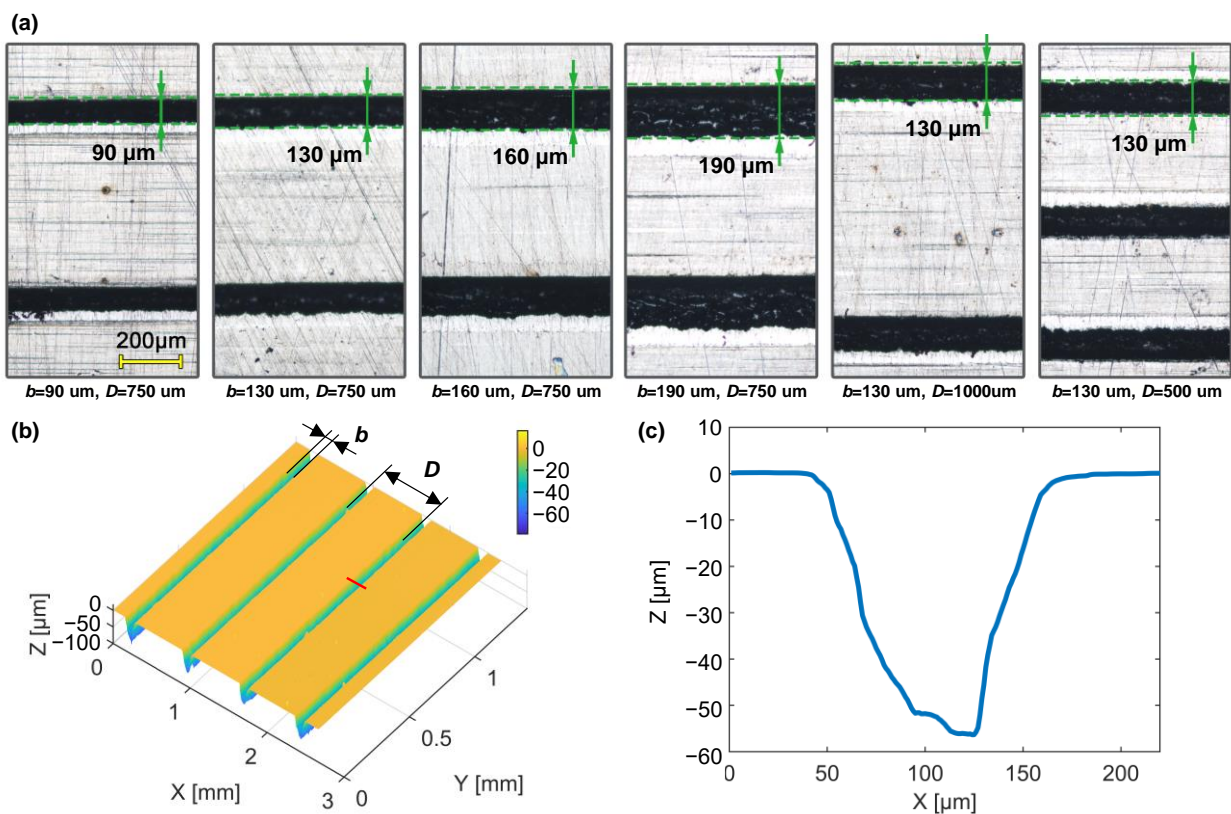
Figure 2. (**a**) Samples with different groove widths *b* and inter-groove distances *D*; (**b**) Surface profile of sample; (**c**) line profile of sample with *b* = 130 μm and *D* = 750 μm.
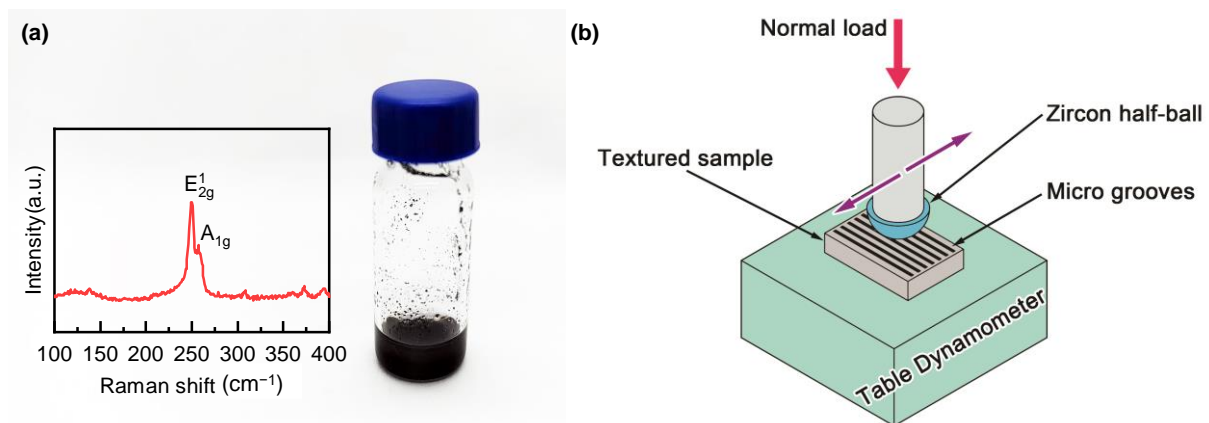
Figure 3. (**a**) Solution of WSe_2 and Raman test result of the WSe_2; (**b**) schematic of sliding tribological tester.

Then, the dried WSe_2 was mixed with a small amount of acetone to create a thick paste. For filling the grooves with the solid lubricant, the WSe_2 flake paste was smeared on the textured surface and scratched with a thin aluminum card (Figure 1). Finally, the sample was dried in the air for 30 min at room temperature. Once the acetone was totally volatilized, the surface was scratched again to remove the residual WSe_2. The sizes of WSe_2 flakes were observed using SEM, which could provide clearer geometrical information than the optical microscope. The influence of different sizes of WSe_2 flakes on friction reduction was investigated in the later section.

3. Experimental Setup

Reciprocating sliding tests were performed using a homemade sliding tribological tester as shown in Figure 3b that comprises a linear motion slider (PDV, PP110-50), a 3 axis high precision piezoelectric sensor (SINOCERA, CL-YD-3302), quasi-static charge amplifier (KISTLER 5015), data acquisition system (SINOCERA, YE6231), and a computer. The force measurement had been calibrated in advance. The friction force and normal force were recorded and analyzed to output the real-time CoF.

A 6 mm half-ball zircon is selected as the other friction pair material used in the sliding tests to form a "ball-on-disk" contact. The sliding speed for each test was 10 mm/s, the sliding distance was 15 mm, and the sliding direction was perpendicular to the micro grooves. The normal load was 3.5 N. Reciprocating sliding tests were performed separately under dry and WSe_2 flake-filled conditions. Tests on non-textured samples were also performed for reference.

4. Results and Discussion

4.1. Results of Dry Sliding

The micro grooves' effect under the dry condition has been investigated for comparison. The average CoF for the non-textured case (NT), and groove width b = 90 μm, 130 μm, 160 μm, 200 μm are plotted, respectively, as shown in Figure 4a, which shows the CoF regarding different groove widths. With the increase in groove width, the CoF reaches the lowest value on the groove width b = 130 μm, then rises gradually with b = 160 and 200 μm. However, the CoF is lower in textured cases than in the non-textured case (NT). Figure 4b shows the CoF regarding the different densities of grooves, and the average CoF are plotted, respectively, for the non-textured case (NT) and textured cases with inter-groove distance D = 500 μm, 750 μm, and 1000 μm. The CoF declines continuously with the decrease in the inter-groove space (the increase in micro groove density).
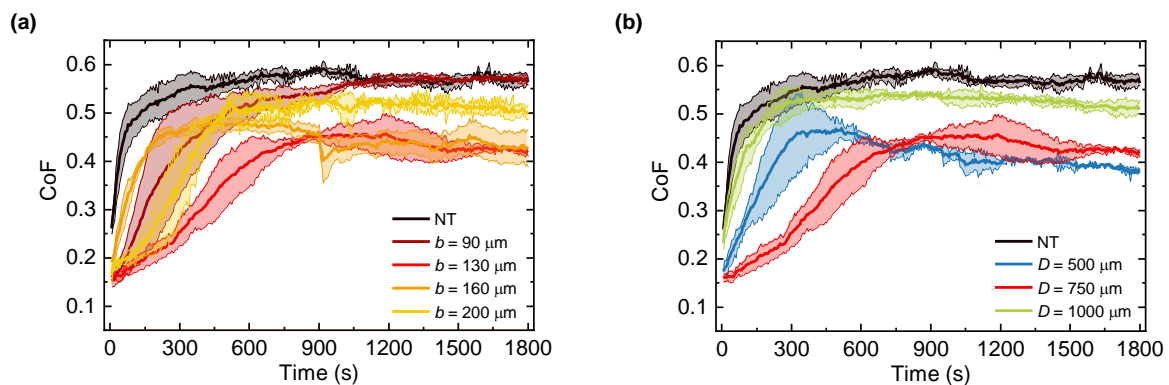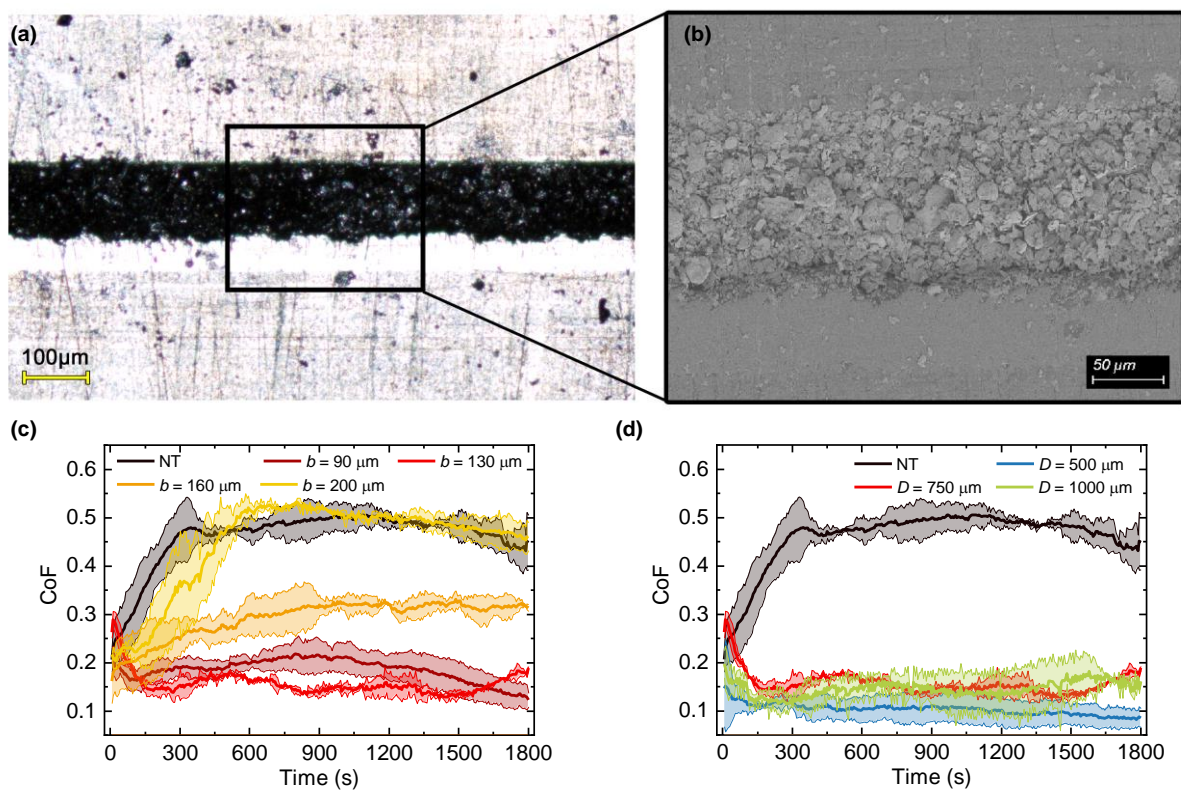

Figure 4. (**a**) CoF for different groove widths and (**b**) CoF for different inter-groove distances.

Compared with the non-textured case (NT), the CoF can be reduced by a maximum of about 20 % with the groove width b = 130 μm. Further, the CoF decreases gradually with higher groove densities on the premise that the width of the groove is constant.

4.2. Results of Solid Lubrication Friction

Reciprocating sliding tests were conducted on the textured samples with WSe_2 flake-filled micro grooves in order to investigate the synergetic effects of micro-texture and layered lubricating material. For comparison, the non-textured sample (NT) was processed in the same procedures as the textured samples. A small amount of the WSe_2 flakes were left on the non-textured surface. Figure 5a,b show a textured surface (b = 130 μm) with the lubricant filling before the sliding test. The groove was fully filled using the flakes of WSe_2, and a few WSe_2 flakes remained on the non-textured surface.

Figure 5. (a) Enlarged and (b) SEM of the micro groove with width $b = 130$ μm; (c) CoF for different groove widths filled with WSe$_2$ flakes, and (d) CoF for different inter-groove distances filled with WSe$_2$ flakes.

Figure 5c compares the CoF regarding different groove widths filled with WSe$_2$ flakes, and all textured samples vary in groove width b with a constant inter-groove distance $d = 750$ μm. For the non-textured case (NT), the CoF is around 0.45~0.5 after 300 s, which is reduced slightly compared to the non-textured case in dry sliding. For the textured samples filled with WSe$_2$ flakes, the CoF drops dramatically to lower than 0.2 when the groove width $b = 90$ μm and 130 μm. Then, with the increase in groove width, the CoF rises back to 0.45 sharply ($b = 200$ μm). Figure 5d shows the CoF regarding the different densities of micro grooves filled with WSe$_2$ flakes. For the textured cases, with the groove width $b = 130$ μm, the CoF can be lower than 0.2. However, it is still noticeable that the denser grooves bring more reduction in CoF, as the lowest CoF is around 0.1 at $D = 500$ μm.

In addition, the influence of the size of WSe$_2$ flakes on synergetic effects was investigated. The texture remains constant for the cases concerning the effects of WSe$_2$ flake size, the groove width $b = 130$ μm, and inter-groove space $D = 500$ μm. Three different sizes of WSe$_2$ flakes were used in the sliding tests, as shown in Figure 6b–d. In Figure 6b, the size of the WSe$_2$ flakes is around 40 μm on average, and a few WSe$_2$ flakes with a larger dimension (>80 μm) can be observed. Figure 6c and 6d shows the flakes with an average size of around 30 μm and 20 μm, respectively. For those two cases, the size is more even for the WSe$_2$ flakes. As shown in Figure 6a, the small size (20 μm) of the WSe$_2$ flakes shows the largest reduction in friction compared to the medium size (30 μm) and large size (40 μm). Figure 6e shows an image of a textured surface with large size WSe$_2$ flakes, and it is apparent that the wear mark is clear and clean. The WSe$_2$ flakes were pushed to the end side of the wear mark, which implies that there very few WSe$_2$ flakes are involved in the sliding contact. It should be stated that all the sliding tests regarding groove widths and densities that were shown in previous sections used the WSe$_2$ flakes with the small flake size.
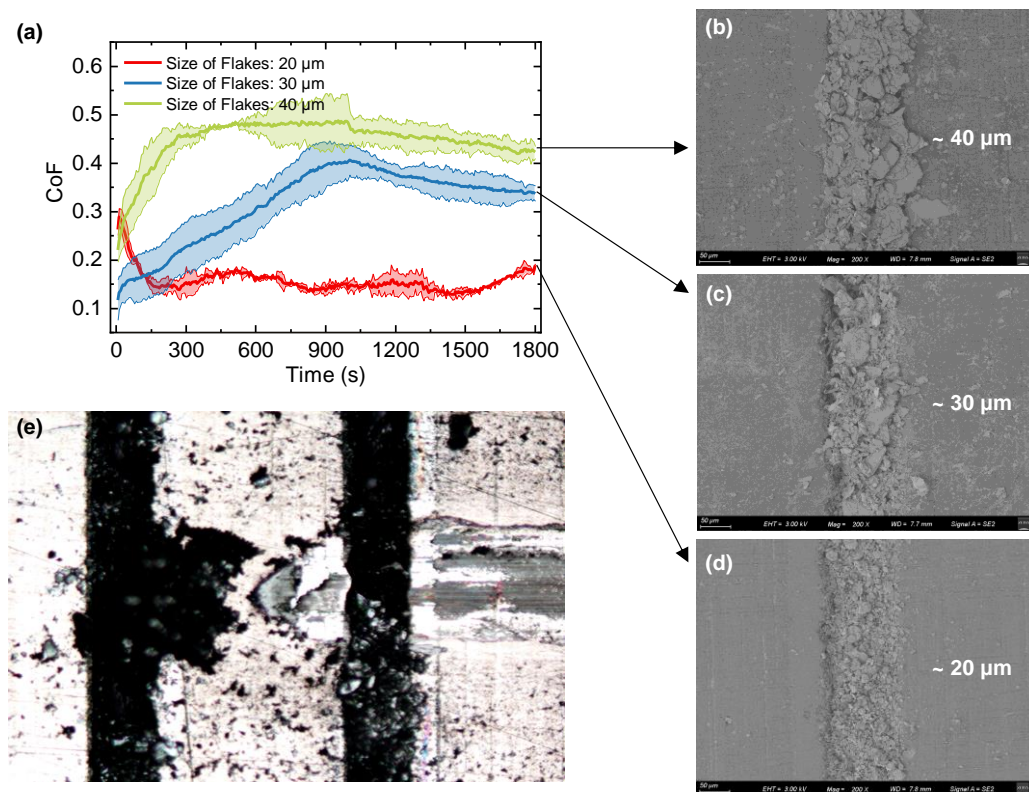
Figure 6. (**a**) CoF for different WSe$_2$ flake sizes; (**b**) large size, (**c**) medium size and (**d**) small size of WSe$_2$ flakes filled in the micro groove; (**e**) image of a textured surface with large size (40 μm) of WSe$_2$ flakes.

In summary, when the grooves were filled with the WSe$_2$ flakes, the CoF was reduced dramatically compared to the cases with micro grooves only. Multiple mechanisms are associated with the significant CoF reduction. A surface with micro grooves filled with WSe$_2$ flakes makes use of both texturing and layered materials' advantages, as the surface texture reduces the contact area and traps debris while the layered materials lubricate the sliding contact [9,46]. The micro groove stores the WSe$_2$ flakes and continuously brings them to the sliding contact area to form the lubricant film. In terms of the influences of texture geometrical features, the width of the micro groove shows a noticeable impact on friction reduction, such that the optimal groove width $b = 130$ μm was identified in this study experimentally for both dry and WSe$_2$ flake-filled conditions. The change trends for CoF regarding groove widths are similar for both dry and WSe$_2$ flake-filled conditions, as shown in Figures 4a and 5c, which implies the mechanism associated with optimal groove width highly relates to the contact condition and friction behaviour of dry sliding. Furthermore, the case with denser micro grooves brings a greater reduction in CoF for both dry and WSe$_2$ flake-filled conditions. A possible explanation for this is that, with more grooves on the surface, the WSe$_2$ flakes have more chances to be transferred to the non-textured area to form a lubricant film. Moreover, we also found that the CoF reduction greatly depends on the size of the flakes in the grooves.

5. Conclusions

In this study, the texture geometrical features' influence on the synergetic effects of the surface texture and solid lubricant was investigated. Micro grooves with different widths and numbers were fabricated on the metal sample surface, and the grooves were filled with micro WSe$_2$ flakes. Reciprocating sliding tests were performed for both dry and WSe$_2$ flake-filled grooves under a ball-on-disk contact condition. The following conclusions can be drawn:

- In the dry sliding, the experimental results confirm the CoF reduction due to micro grooves on the surface, and that the CoF could be reduced by 20% at maximum compared to the non-textured case;
- The combination of micro grooves and WSe_2 micro flakes could further reduce the CoF significantly, and the CoF could be reduced by 80% compared to non-textured cases;
- The optimal groove width ($b = 130$ μm) for both dry and WSe_2 flake-filled conditions was determined from the experimental results. The density of the micro grooves has a positive relationship with the CoF reduction for both dry and WSe_2 flake-filled conditions;
- According to the SEM observation, WSe2 flakes with different sizes were applied in the test. The size of WSe_2 flakes is important for the synergetic effects of micro grooves and WSe_2 flakes. An average size of the WSe_2 flake of 20 μm leads to the lowest CoF in the sliding tests.

References

1. Sattari Baboukani, B.; Ye, Z.; Reyes, K.G.; Nalam, P.C. Prediction of Nanoscale Friction for Two-Dimensional Materials Using a Machine Learning Approach. *Tribol. Lett.* **2020**, *68*, 27. [CrossRef]
2. Lee, J.H.; Cho, D.-H.; Park, B.H.; Choi, J.S. Nanotribology of 2D materials and their macroscopic applications. *J. Phys. D Appl. Phys.* **2020**, *53*, 393001. [CrossRef]
3. Priest, M.; Taylor, C.M. Automobile engine tribology—Approaching the surface. *Wear* **2000**, *241*, 193–203. [CrossRef]
4. Ryk, G.; Etsion, I. Testing piston rings with partial laser surface texturing for friction reduction. *Wear* **2006**, *261*, 792–796. [CrossRef]
5. Vlǎdescu, S.-C.; Olver, A.V.; Pegg, I.G.; Reddyhoff, T. Combined friction and wear reduction in a reciprocating contact through laser surface texturing. *Wear* **2016**, *358–359*, 51–61. [CrossRef]
6. Manu, B.R.; Gupta, A.; Jayatissa, A.H. Tribological Properties of 2D Materials and Composites—A Review of Recent Advances. *Materials* **2021**, *14*, 1630. [CrossRef]
7. Holmberg, K.; Erdemir, A. Influence of tribology on global energy consumption, costs and emissions. *Friction* **2017**, *5*, 263–284. [CrossRef]
8. Freschi, M.; Paniz, A.; Cerqueni, E.; Colella, G.; Dotelli, G. The Twelve Principles of Green Tribology: Studies, Research, and Case Studies—A Brief Anthology. *Lubricants* **2022**, *10*, 129. [CrossRef]
9. Rosenkranz, A.; Costa, H.L.; Baykara, M.Z.; Martini, A. Synergetic effects of surface texturing and solid lubricants to tailor friction and wear—A review. *Tribol. Int.* **2021**, *155*, 106792. [CrossRef]
10. Zimmerman, J.H.; Guleryuz, C.G.; Krzanowski, J.E. Fabrication and tribological properties of titanium nitride coatings incorporating solid lubricant microreservoirs. *Surf. Coat. Technol.* **2008**, *202*, 2023–2032. [CrossRef]
11. Ze, W.; Jianxin, D.; Yang, C.; Youqiang, X.; Jun, Z. Performance of the self-lubricating textured tools in dry cutting of Ti-6Al-4V. *Int. J. Adv. Manuf. Technol.* **2012**, *62*, 943–951. [CrossRef]
12. Arenas, M.A.; Ahuir-Torres, J.I.; García, I.; Carvajal, H.; de Damborenea, J. Tribological behaviour of laser textured Ti6Al4V alloy coated with MoS2 and graphene. *Tribol. Int.* **2018**, *128*, 240–247. [CrossRef]
13. Guo, Y.; Zhou, X.; Lee, K.; Yoon, H.C.; Xu, Q.; Wang, D. Recent development in friction of 2D materials: From mechanisms to applications. *Nanotechnology* **2021**, *32*, 312022–312036. [CrossRef] [PubMed]

14. Song, F.; Yang, X.; Dong, W.; Zhu, Y.; Wang, Z.; Wu, M. Research and prospect of textured sliding bearing. *Int. J. Adv. Manuf. Technol.* **2022**, *121*, 1–25. [CrossRef]
15. Fuseini, M.; Zaghloul, M.M.Y. Investigation of Electrophoretic Deposition of PANI Nano fibers as a Manufacturing Technology for corrosion protection. *Prog. Org. Coat.* **2022**, *171*, 107015. [CrossRef]
16. Fuseini, M.; Zaghloul, M.M.Y. Statistical and qualitative analyses of the kinetic models using electrophoretic deposition of polyaniline. *J. Ind. Eng. Chem.* **2022**, *113*, 475–487. [CrossRef]
17. Suh, N.P.; Mosleh, M.; Howard, P.S. Control of friction. *Wear* **1994**, *175*, 151–158. [CrossRef]
18. Yan, D.; Qu, N.; Li, H.; Wang, X. Significance of Dimple Parameters on the Friction of Sliding Surfaces Investigated by Orthogonal Experiments. *Tribol. Trans.* **2010**, *53*, 703–712. [CrossRef]
19. Youqiang, X.; Jianxin, D.; Xiuting, F.; Sheng, Y. Effect of laser surface texturing on Si3N4/TiC ceramic sliding against steel under dry friction. *Mater. Des.* **2013**, *52*, 234–245.
20. Sun, Q.; Hu, T.; Fan, H.; Zhang, Y.; Hu, L. Dry sliding wear behavior of TC11 alloy at 500°C: Influence of laser surface texturing. *Tribol. Int.* **2015**, *92*, 136–145. [CrossRef]
21. Kumar, M.; Ranjan, V.; Tyagi, R. Effect of Shape, Density, and an Array of Dimples on the Friction and Wear Performance of Laser Textured Bearing Steel under Dry Sliding. *J. Mater. Eng. Perform.* **2020**, *29*, 2827–2838. [CrossRef]
22. Borghi, A.; Gualtieri, E.; Marchetto, D.; Moretti, L.; Valeri, S. Tribological effects of surface texturing on nitriding steel for high-performance engine applications. *Wear* **2008**, *265*, 1046–1051. [CrossRef]
23. Shimizu, J.; Nakayama, T.; Watanabe, K.; Yamamoto, T.; Onuki, T.; Ojima, H.; Zhou, L. Friction characteristics of mechanically microtextured metal surface in dry sliding. *Tribol. Int.* **2020**, *149*, 105634. [CrossRef]
24. Zhu, Y.; Chen, J.; Du, J.; Fan, Y.; Zheng, J. Tribological behavior of laser textured nodular cast iron surface. *Ind. Lubr. Tribol.* **2019**, *71*, 949–955. [CrossRef]
25. Hichri, Y.; Cerezo, V.; Do, M.T.; Zahouani, H. Effect of particles' characteristics and road surface's texture on the tire/road friction. *Surf. Topogr. Metrol. Prop.* **2018**, *6*, 034014. [CrossRef]
26. Yu, A.; Niu, W.; Hong, X.; He, Y.; Wu, M.; Chen, Q.; Ding, M. Influence of tribo-magnetization on wear debris trapping processes of textured dimples. *Tribol. Int.* **2018**, *121*, 84–93. [CrossRef]
27. Rosenkranz, A.; Reinert, L.; Gachot, C.; Mücklich, F. Alignment and wear debris effects between laser-patterned steel surfaces under dry sliding conditions. *Wear* **2014**, *318*, 49–61. [CrossRef]
28. Wang, M. The tribological performance of engineered micro-surface topography by picosecond laser on PEEK. *Ind. Lubr. Tribol.* **2019**, *72*, 172–179. [CrossRef]
29. Scharf, T. Low friction coatings. In *Handbook of Lubrication and Tribology*; CRC Press: Boca Raton, FL, USA, 2012.
30. Scharf, T.; Prasad, S. Solid lubricants: A review. *J. Mater. Sci.* **2013**, *48*, 511–531. [CrossRef]
31. Sahoo, S. Self-lubricating composites with 2D materials as reinforcement: A new perspective. *Reinf. Plast.* **2021**, *65*, 101–103. [CrossRef]
32. Voevodin, A.A.; Bultman, J.; Zabinski, J.S. Investigation into three-dimensional laser processing of tribological coatings. *Surf. Coat. Technol.* **1998**, *107*, 12–19. [CrossRef]
33. Rapoport, L.; Moshkovich, A.; Perfilyev, V.; Lapsker, I.; Halperin, G.; Itovich, Y.; Etsion, I. Friction and wear of MoS2 films on laser textured steel surfaces. *Surf. Coat. Technol.* **2008**, *202*, 3332–3340. [CrossRef]
34. Jianxin, D.; Wenlong, S.; Hui, Z. Design, fabrication and properties of a self-lubricated tool in dry cutting. *Int. J. Mach. Tools Manuf.* **2009**, *49*, 66–72. [CrossRef]
35. Hu, T.; Zhang, Y.; Hu, L. Tribological investigation of MoS2 coatings deposited on the laser textured surface. *Wear* **2012**, *278–279*, 77–82. [CrossRef]
36. Reinert, L.; Lasserre, F.; Gachot, C.; Grutzmacher, P.; MacLucas, T.; Souza, N.; Mucklich, F.; Suarez, S. Long-lasting solid lubrication by CNT-coated patterned surfaces. *Sci. Rep.* **2017**, *7*, 42873. [CrossRef]
37. Meng, R.; Deng, J.; Liu, Y.; Duan, R.; Zhang, G. Improving tribological performance of cemented carbides by combining laser surface texturing and W-S-C solid lubricant coating. *Int. J. Refract. Met. Hard Mater.* **2018**, *72*, 163–171. [CrossRef]
38. Zhang, H.; Hua, M.; Dong, G.; Zhang, D.; Chin, K.-S. A mixed lubrication model for studying tribological behaviors of surface texturing. *Tribol. Int.* **2016**, *93*, 583–592. [CrossRef]
39. Zhang, H.; Zhang, D.Y.; Hua, M.; Dong, G.N.; Chin, K.S. A Study on the Tribological Behavior of Surface Texturing on Babbitt Alloy under Mixed or Starved Lubrication. *Tribol. Lett.* **2014**, *56*, 305–315. [CrossRef]
40. Tang, W.; Zhou, Y.; Zhu, H.; Yang, H. The effect of surface texturing on reducing the friction and wear of steel under lubricated sliding contact. *Appl. Surf. Sci.* **2013**, *273*, 199–204. [CrossRef]
41. Papadopoulos, C.I.; Efstathiou, E.E.; Nikolakopoulos, P.G.; Kaiktsis, L. Geometry Optimization of Textured Three-Dimensional Micro- Thrust Bearings. *J. Tribol.* **2011**, *133*. [CrossRef]
42. Zaghloul, M.M.Y.; Zaghloul, M.Y.M.; Zaghloul, M.M.Y. Experimental and modeling analysis of mechanical-electrical behaviors of polypropylene composites filled with graphite and MWCNT fillers. *Polym. Test.* **2017**, *63*, 467–474. [CrossRef]
43. Zaghloul, M.Y.; Zaghloul, M.M.Y.; Zaghloul, M.M.Y. Influence of Stress Level and Fibre Volume Fraction on Fatigue Performance of Glass Fibre-Reinforced Polyester Composites. *Polymers* **2022**, *14*, 2662. [CrossRef]

44. Huang, Y.; Pan, Y.-H.; Yang, R.; Bao, L.-H.; Meng, L.; Luo, H.-L.; Cai, Y.-Q.; Liu, G.-D.; Zhao, W.-J.; Zhou, Z. Universal mechanical exfoliation of large-area 2D crystals. *Nat. Commun.* **2020**, *11*, 1–9.

45. Sun, J.; Wang, Y.; Guo, S.; Wan, B.; Dong, L.; Gu, Y.; Song, C.; Pan, C.; Zhang, Q.; Gu, L.; et al. Lateral 2D WSe2 p-n Homojunction Formed by Efficient Charge-Carrier-Type Modulation for High-Performance Optoelectronics. *Adv. Mater.* **2020**, *32*, e1906499. [CrossRef]

46. Schäfer, C.; Reinert, L.; MacLucas, T.; Grützmacher, P.; Merz, R.; Mücklich, F.; Suarez, S. Influence of Surface Design on the Solid Lubricity of Carbon Nanotubes-Coated Steel Surfaces. *Tribol. Lett.* **2018**, *66*, 89. [CrossRef]